H_2O involvement rather than from reduced anion entry (i.e. N_3^-, ClO_4^-, $CF_3SO_3^-$). Clearly the activation energy for the "turnaround" process is higher than that for N_3^- entry, which might suggest different transition states. However, whereas recapture of thiocyanate requires little separation of SCN^- from Co(III) and therefore probably only a minor contribution from the surrounding solvent, the capture of N_3^- contains contributions from both the formation of the ion pair and subsequent coordination to Co. It is likely that K_{IP} increases with decreasing temperature, whereas the release of N_3^- from the ion pair will be made more difficult since this will involve considerable desolvation of the N_3^- ion (breaking of H-bonds). In our view it is these opposing tendencies that lead to the constant incorporation of CoN_3^{2+} at the two temperatures.

In summary, the amount of isomerization $CoSCN^{2+} \rightarrow CoNCS^{2+}$ is only slightly affected by the presence of N_3^- (and other anions) in the immediate solvent cage, and entry of N_3^- from $Co(NH_3)_4(NH_2)\text{---}X^{n-1},N_3^-$ is little influenced by the presence or absence of isomerization; H_2O is the major entering group when isomerization is absent or when N_3^- entry is reduced. Likewise, only the stereochemistry of H_2O entry is significantly affected by such processes (and then only by isomerization and not by N_3^- entry); the stereochemistry of anion entry (CoN_3^{2+}) is little affected by isomerization ($CoNCS^{2+}$) and the stereochemistry of the isomerized product is not at all affected by the presence of other anions. Also, isomerization is distinguished from N_3^- entry in an energetic sense.

Such facts imply the coupling of H_2O entry with N_3^- and NCS^- entry, but with the last two processes being largely uncoupled. However, all three processes must be competitive in the sense that they happen at the same time; they do not happen in a stepwise fashion with the appearance of a stable intermediate following NCS^- entry and before N_3^- entry. The results would suggest the existence of a number of intermediates, each containing entering groups in stereochemical positions closely related to those adopted in the final product. A relatively important member is

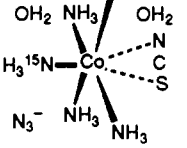

with N_3^- distant in a stereochemical sense from thiocyanate. Whether such intermediates contain truly five-coordinate cobalt(III) species, with complete breaking of the Co–SCN bond before entry of the sixth ligand, remains unknown. If bond breaking is complete, then the lifetime of these intermediates is insufficient to relocate thiocyanate into different stereochemical positions. If relocation of the other ion-paired entering groups or of H_2O from the second coordination sphere is on a similar time scale, then the five-coordinate species do not exist long enough to be observed by the type of experiments outlined here. If this is so in a general sense for all CoX^{n+} reactants (i.e. there is nothing special about the $CoSCN^{2+}$ substrate), then the lifetime of all such five-coordinate species[30] in the base hydrolysis reaction will be insufficient to allow major stereochemical adjustments within the second coordination sphere[31] and this type of experimental distinction between stepwise (e.g. $S_N1(CB)$ or I_d) and concerted ($S_N1(CB)$ or I_a) mechanisms[29] disappears.

Registry No. $[Co(NH_3)_5SO_4]HSO_4$, 49732-36-7; $[Co(NH_3)_5F](NO_3)_2$, 14240-02-9; $[Co(NH_3)_5OPO(O^nBu)_2](ClO_4)_2$, 123812-51-1; $[Co(NH_3)_5OPO(OMe)_2](ClO_4)_2$, 90568-50-6; $[Co(NH_3)_5NCS]Cl_2$, 15244-70-9; $[Co(NH_3)_5Cl]Cl_2$, 13859-51-3; $[Co(NH_3)_5Br]Br_2$, 14283-12-6; $[Co(NH_3)_5I]Cl_2$, 14972-82-8; $[Co(NH_3)_5NO_3]^{2+}$, 15077-44-1; $[Co(NH_3)_5CH_3SO_3](ClO_4)_2$, 76024-71-0; $[Co(NH_3)_5ClO_4](ClO_4)_2$, 18042-14-3; $[Co(NH_3)_5OSO_2CF_3](CF_3SO_3)_2$, 75522-50-8; $[Co(NH_3)_5Me_2SO](ClO_4)_3$, 51667-94-8; $[Co(NH_3)_5OP(OMe)_3](ClO_4)_3$, 15041-41-5; $[Co(NH_3)_5SCN]Br_2$, 35672-90-3; CoN_3^{2+}, 14403-83-9; $CoOH_2^{3+}$, 14403-82-8; *trans*-$[Co(NH_3)_4(^{15}NH_3)Br]Br_2$, 123812-52-2; *trans*-$[Co(NH_3)_4(^{15}NH_3)Br](CF_3SO_3)_2$, 123812-54-4; *trans*-$[Co(NH_3)_4(^{15}NH_3)Cl]^{2+}$, 88537-87-5; *trans*-$[Co(NH_3)_4(^{15}NH_3)NO_3]^{2+}$, 123834-34-4; *trans*-$[Co(NH_3)_4(^{15}NH_3)OSO_2CF_3](CF_3SO_3)_2$, 97348-29-3; *trans*-$[Co(NH_3)_4(^{15}NH_3)SCN]Br_2$, 123812-59-9; *trans*-$[Co(NH_3)_4(^{15}NH_3)F](CF_3CO_2)_2$, 123812-56-6; *trans*-$[Co(NH_3)_4(^{15}NH_3)SO_4]ClO_4$, 123812-58-8; *trans*-$[Co(NH_3)_4(^{15}NH_3)Me_2SO](ClO_4)_3$, 88642-41-5; *trans*-$[Co(NH_3)_4(^{15}NH_3)OP(OMe)_3](ClO_4)_3$, 97251-80-4.

(30) Rotzinger has suggested the existence of a "hexacoordinate cobalt(III) intermediate" following Co–X bond rupture and before entry of adjacent groups.[2] We find it hard to visualize what this might be other than a tight ion pair, but he assures us that he has carried out SCF calculations supporting their existence (private communication). We have no evidence to quantify the lifetime of any intermediate subsequent to breaking the Co–X bond, but the implications from the stereochemical results presented here infer that it must be short relative to major readjustments in the second coordination sphere.

(31) This would require solvent-separated ion pairs to give $CoOH_2^{3+}$, rather than CoN_3^{2+}.

(32) Since a transition state, intermediate, or indeed any configuration is a point on the potential energy surface of a reaction, all contributions to this energy surface, including those from the immediate surroundings, must be taken into consideration.

Contribution from the Laboratoire de Chimie Quantique, E.R. 139 du CNRS, Université Louis Pasteur, 4 rue Blaise Pascal, F-67000 Strasbourg, France

Theoretical Study of the Electron Density in Iron(II) Porphyrin Bis(water)

Marie-Madeleine Rohmer

Received January 23, 1989

Ab initio SCF and CI calculations are reported for four different electronic configurations of the high-spin six-coordinate iron(II) porphyrin bis(water) molecule considered as a model for iron(II) tetraphenylporphyrin bis(tetrahydrofuran). The $^5B_{2g}$ and ^5E_g states are the lowest ones in energy and turn out to be nearly degenerate at both levels of theory. The ground-state configuration of iron(II) tetraphenylporphyrin bis(tetrahydrofuran) is assigned as ^5E_g on the basis of a comparison between the theoretical electron deformation density maps and the experimental ones.

Introduction

Recently, Lecomte et al. reported the electron density distribution in iron(II) tetraphenylporphyrin bis(tetrahydrofuran), $FeTPP(THF)_2$, derived from low-temperature X-ray diffraction data, and they attempted to determine the ground state of this high-spin complex.[1] They came to the conclusion that "a further analysis of the electron distribution determined in this study and the corresponding ground-state assignment requires comparison with parallel theoretical calculations. No such calculations are available as yet for $Fe^{II}(THF)_2TPP$." We report here the results obtained from SCF and CI calculations for the different states of the iron(II) porphyrin bis(water) complex $Fe^{II}P(H_2O)_2$ (P = porphine dianion) (Figure 1) considered as a model of the above-mentioned iron(II) porphyrin bis(tetrahydrofuran).[2] In

(1) Lecomte, C.; Blessing, R. H.; Coppens, P.; Tabard, A. *J. Am. Chem. Soc.* **1986**, *108*, 6942.

(2) Reed, C. A.; Mashiko, T.; Scheidt, W. R.; Spartalian, K.; Lang, G. *J. Am. Chem. Soc.* **1980**, *102*, 2302.

0020-1669/89/1328-4574$01.50/0

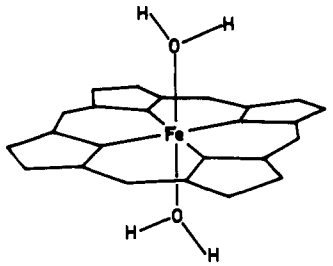

Figure 1. $FeP(H_2O)_2$ model.

Table I. d-Orbital Occupations and Total Energies (in au and Relative to −2393) for the Different Quintet States of $FeP(H_2O)_2$

	formal occupation no.					
state	x^2-y^2	z^2	xz, yz	xy	E(SCF)	E(CI)
$^5B_{2g}$	1	1	2	2	0.199	0.217
$^5A_{1g}$	1	2	2	1	0.176	0.191
$^5B_{1g}$	2	1	2	1	0.136	0.149
^5E_g	1	1	3	1	0.197	0.217

a previous study, we have computed the electron deformation density maps for the $^3A_{2g}$ and ^3E_g states of the four-coordinate iron(II) porphyrin FeP from ab initio calculations at the CI level.[3] These theoretical maps turn out to be a useful tool for the discussion of the ground state of FeP and have been used by Tanaka et al. in their study of the electron density of (*meso*-tetraphenylporphinato)iron(II), FeTPP.[4] In fact this first experimental study of FeTPP did not provide conclusive results and a new experimental study has been undertaken recently.[5] A comparison of the new experimental maps with the theoretical maps now leads to the assignment of the $^3A_{2g}$ state as the leading contributor to the ground state of the isolated complex, in agreement with our previous conclusion that this state must be the ground state.[3] The idea that collaborative techniques (experimental X-ray analysis vs theoretical calculations) are extremely useful in the study of metalloporphyrins has provided the impetus for the present work.

Calculations

Ab initio SCF calculations were carried out with the ASTERIX system of programs[6] on $FeP(H_2O)_2$ with the following basis sets: (14,9,6) contracted to [6,4,3] for iron, (9,5) contracted to [3,2] for the first-row atoms, and (4) contracted to [2] for hydrogen.[7] The contracted basis set is minimal for the inner shells, double-ζ for the valence shells, and triple-ζ for the 4s and 3d shells of iron. The porphyrin ligand was assumed to be planar, and the bond lengths were taken from the experimental geometry of $FeTPP(THF)_2$[1] with Fe–N = 2.066 Å and Fe–O = 2.292 Å. The iron atom sits in the porphyrin plane and the water molecules (used to mimic the THF ligands) eclipse two opposite meso carbon atoms. The overall symmetry of the molecule is D_{2h}, but since the wave function deviates only slightly from D_{4h}, we shall use the D_{4h} notations to label the electronic states.

First, an open-shell SCF calculation was carried out for each of the quintet electronic states corresponding to the different occupations of the d orbitals (Table I). Next, a CI calculation was carried out for each electronic state with the corresponding SCF wave function as reference wave function. All single and double excitations relative to the reference state were considered within a set of 30 active orbitals. This set was made of the five d orbitals of the metal together with 25 unoccupied orbitals, which were chosen from the SCF virtual orbitals having the largest iron character. Unitary transformations were performed on the occupied and unoccupied space in order to maximize the weight of the iron atom in the active orbitals. These CI calculations were carried out with the CI program developed originally by Brooks and Schaefer[8] using the graphical unitary group approach.[9]

The electron deformation density distribution—defined as the difference between the molecular electron density distribution and the superposition of spherically averaged atomic distributions (each atom being considered in its ground state)—has been computed from both SCF and CI wavefunctions for the four states considered.

Results and Discussion

Table I gives the SCF and CI energies for the four electronic states of $FeP(H_2O)_2$ under consideration. At the SCF level the states $^5B_{2g}$ and ^5E_g are nearly degenerate (the energy gap being 0.05 eV), with the two states $^5A_{1g}$ and $^5B_{1g}$ appreciably higher in energy (as expected on qualitative grounds). The near degeneracy of the two states $^5B_{2g}$ and ^5E_g is also understandable, since these two states are of the type $(t_{2g})^4(e_g)^2$.

The energy lowering due to CI varies from 0.35 eV for the $^5B_{1g}$ state to 0.54 eV for the ^5E_g state. This lowering is somewhat smaller than the one of 1.0–1.3 eV computed previously for the different states of the four-coordinate iron(II) porphyrin FeP in a CI calculation with the same number of active orbitals.[10] Thus, correlation effects appear less important in the six-coordinate high-spin iron(II) porphyrin bis(water) compared to the other porphyrin systems studied previously,[3,7] a result which is understandable on the basis of the number of electron pairs.

The main conclusion of the CI calculations is that the states ^5E_g and $^5B_{2g}$ remain nearly degenerate at this level. Thus, on energy grounds only, it does not seem possible to decide on the electronic ground state of high-spin six-coordinate iron(II) porphyrins.

As in our previous studies,[3] the deformation density maps computed from SCF and CI wave functions turn out to be nearly identical. This is a consequence of the small changes brought in the electronic distribution by the configuration mixing.[11] Deformation density maps from the CI wave functions in the porphyrin plane are displayed in Figures 2 and 3 for the states $^5B_{2g}$ and ^5E_g of $FeP(H_2O)_2$. This section is particularly well suited for a comparison with the experimental maps because of the various features generated by the metal–nitrogen interaction and by the bonds between the first-row atoms. Furthermore, it is the only one for which the comparison seems possible (since the only other experimental deformation densities reported, namely those in the plane perpendicular to the porphyrin, have not been averaged). The theoretical maps in the region of the pyrrole ring (Figure 2) do not allow us to discriminate between the two states. The corresponding electron density distributions are rather similar to the one displayed in the experimental map. In particular, the C_β–C_β bond of the pyrrole ring shows a peak more pronounced than those of the other pyrrole bonds, indicating a larger double-bond character.

The comparison of the experimental and theoretical maps for the region of the iron and nitrogen atoms is shown in Figure 3. For the $^5B_{2g}$ state the theoretical map displays four important peaks of accumulation along the bisectors of the Fe–N bonds, which are easy to interpret, since they represent excess population in the d_{xy} orbital. On the other hand, for the ^5E_g state one finds no accumulation of density along the bisector direction, but a slight accumulation of density (0.3 e Å^{-3}) is rather observed along the Fe–N bonds very close (0.3 Å) to the metal. This peak is separated from the nitrogen lone-pair accumulation by a saddle point of the density distribution, slightly negative (−0.05 e Å^{-3}) on the computed map (Figure 3b), slightly positive (+0.10 e Å^{-3}) on the experimental and model maps (Figure 3c,d). Outside a sphere

(3) Rohmer, M. M. *Chem. Phys. Lett.* **1985**, *116*, 44.
(4) Tanaka, K.; Elkaim, E.; Liang Li; Zhu Nai Jue; Coppens, P.; Landrum, J. *J. Chem. Phys.* **1986**, *84*, 6969.
(5) Coppens, P. In *Computational Chemistry. The Challenge of d and f Electrons*; Salahub, D. R., Zerner, M. C., Eds; ACS Symposium Series; American Chemical Society: Washington, DC, 1989, in press.
(6) Bénard, M.; Dedieu, A.; Demuynck, J.; Rohmer, M. M.; Strich, A.; Wiest, R.; Veillard, A. "ASTERIX: a System of Programs", unpublished work.
(7) For a complete description of the basis sets used, see: Rohmer, M. M. In *Quantum Chemistry: The Challenge of Transition Metals and Coordination Chemistry*; Veillard, A., Ed.; NATO ASI Series 176; Reidel: Dordrecht, The Netherlands, 1986; p 377.
(8) Brooks, B. R.; Schaefer, H. F. *J. Chem. Phys.* **1979**, *70*, 5092.
(9) (a) Paldus, J. *Theor. Chem. Adv. Perspect.* **1976**, *2*, 131. (b) Shavitt, I. *Int. J. Quant. Chem. Symp.* **1977**, *11*, 131.
(10) Rohmer, M. M. Unpublished results.
(11) Baert, F.; Guelzim, A.; Poblet, J. M.; Wiest, R.; Demuynck, J.; Bénard, M. *Inorg. Chem.* **1986**, *25*, 1830.

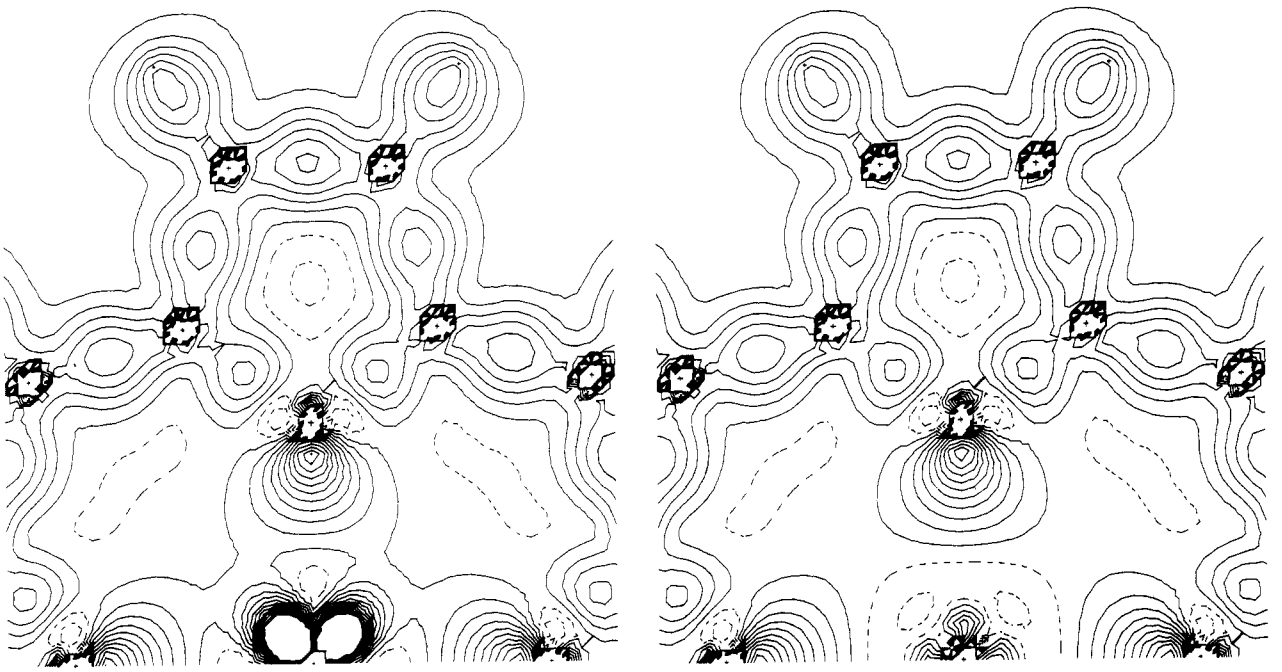

Figure 2. Deformation density maps in the porphyrin plane, showing the pyrrole ring: (a, left) and (b, right) computed respectively for the $^5B_{2g}$ and the ^5E_g states of $FeP(H_2O)_2$. The contour interval is 0.10 e Å^{-3} and negative contours are dashed.

of ca. 0.2 Å around the iron atom, the metal contribution to the density along the Fe–N directions is given by the $3p_{x,y}$ and the $3d_{x^2-y^2}$ metal orbitals. The Mulliken population analysis of the molecule shows that the population of the contracted Gaussian functions (CGTO's) describing these orbitals has globally decreased by 0.14 e with respect to the superposition of the free atoms. This seems to be in contradiction with the presence of peaks in the vicinity of the metal. However, a more careful investigation of the Mulliken analysis reveals that the variation of the metal population along the x and y axes is not equally distributed in space. The population of the most diffuse CGTO participating in the metal $3d_{x^2-y^2}$ orbital has decreased by 0.21 e with respect to the free atoms. This is consistent with the presence of a depopulated region on the computed map between 0.45 and 0.95 Å from the metal along these directions. On the other hand, the population of the innermost CGTO describing the metal valence shell along x and y, which shows a maximum of density at 0.26 Å from the nucleus, has *increased* by 0.066 e with respect to the promolecule. Due to the influence of σ donation, the electron density populating the $3d_{x^2-y^2}$ metal orbital has therefore been squeezed against the nucleus, giving rise to the four peaks at 0.3 Å from the iron atom.[12] At variance with this situation, a decrease of the electron density along the bisector axes is observed. It coincides with an *expansion* of the d_{xy} orbital and a noticeable decrease of the populations of its CGTO components (except for the most diffuse one, which has increased by only 0.05 e). This explains the origin of the deeper depopulation regions computed at ca. 0.57 Å from the metal.

One can note from the comparison of parts b and c of Figure 3 that the computed density pattern discussed above is similar to the one obtained by Lecomte et al[1] after averaging the observed X-ray density distribution. Moreover, the modelized map obtained from a multipole refinement of the observed distribution (Figure 3d) shows near-quantitative agreement with the theoretical map of Figure 3b, with respect to the peak height (0.25 vs 0.30 e Å^{-3}), the hole depth (−0.2 e Å^{-3} in both cases), and the location of the density pits (0.53 vs 0.57 Å). The main difference comes from the location of the peaks, which are further away from the nucleus compared to the theoretical map (0.5 vs 0.3 Å) and connected to the nitrogen lone pairs by a continuous region of weak accumulation. This diffuse accumulation (0.10 e Å^{-3}) is probably at the origin of the large population estimated for the $d_{x^2-y^2}$ orbital from the refined distribution (1.42 e).

(12) A similar contraction of the valence electron population along the Fe–N axes occurs for the $^5B_{2g}$ state, but the local accumulation resulting from this quantitatively minor reorganization cannot be distinguished from the broad peaks along the bisectors resulting from the full occupation of the d_{xy} orbital.

Table II. Calculated Iron Atom d-Orbital Populations of $FeP(H_2O)_2$ and d-Orbital Occupations Derived from the Multipole Analysis for $Fe(TPP)(THF)_2$ (from Ref 1)

	$^5B_{2g}$	$^5A_{1g}$	$^5B_{1g}$	^5E_g	expt
$d_{x^2-y^2}$	0.99	0.98	1.91	0.99	1.42
d_{z^2}	0.85	1.82	0.85	0.85	1.04
$d_{xz,yz}$	1.90	1.90	1.90	2.90	2.52
d_{xy}	2.05	1.06	1.06	1.06	0.93
total	5.79	5.76	5.72	5.80	5.92

The comparison of the experimental and theoretical maps in the porphyrin plane (Figure 3) indicates without doubt that the ground state should be assigned as ^5E_g. One can see from Table II that the theoretical populations of the metal 3d orbitals do not deviate appreciably from the formal occupation numbers of Table I. Therefore, one could tentatively attribute the high population of the $d_{x^2-y^2}$ orbital derived from the experimental distribution to an incomplete deconvolution of the thermal motion. Thermal vibration could therefore smear out the slight depopulation region located along the Fe–N bonds between the two peaks respectively associated with metal and nitrogen.

The net charge on the iron atom is found to be +2.16 e for the ^5E_g state and +2.13 e for the $^5B_{2g}$ state. For both states, the nitrogen atoms bear a negative charge (−0.90 e) as do the oxygen atoms of the water ligands (−0.76 e). The total charge on the water ligand is slightly negative (−0.05 e).

It is commonly accepted that a moderate π-back-bonding from the metal atom to the porphyrin ligand helps to relieve the charge buildup on the metal atom that results from σ donation. With the π populations of the porphyrin ligand amounting to 26.13 and 26.11 for the ^5E_g and $^5B_{2g}$ states, respectively, the $FeP(H_2O)_2$ system shows indeed a small π charge transfer from the iron to the porphyrin. Since the $d_{xz,yz}$ population is larger for the ^5E_g state than for the $^5B_{2g}$ state, one would expect a larger charge transfer for the former state. This is indeed the case, although the difference is rather small.

In relation to this work, one should mention a theoretical study of the quintet, triplet, and singlet states of diammineiron(II) porphyrin, $Fe^{II}P(NH_3)_2$, by Rawlings et al.[13] Three different

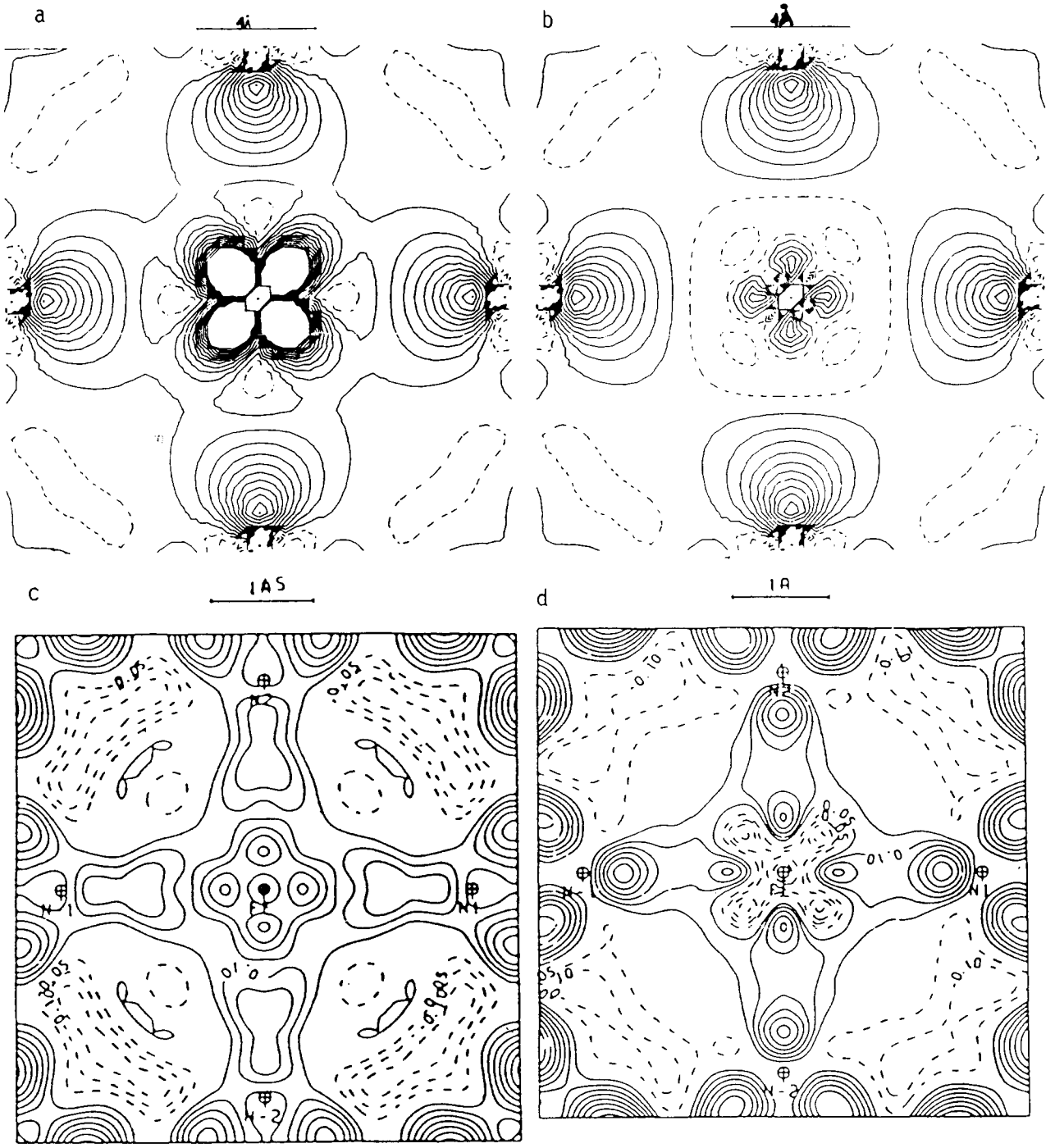

Figure 3. Deformation density maps in the porphyrin plane for the iron and nitrogen region: (a, top left) and (b, top right) computed respectively for the $^5B_{2g}$ and ^5E_g states of $FeP(H_2O)_2$ (contours as in Figure 2); (c, bottom left) averaged X–X map taken from the experimental study on $FeTPP(THF)_2$ (contours at 0.05 e Å^{-3}, zero contour skipped); (d, bottom right) multipole refinement of the distribution observed for $FeTPP(THF)_2$ (contours as in (c)). Maps c and d are reproduced from ref 1 with permission.

high-spin configurations have been considered at the SCF level, namely $^5A_2$ and $^5B_1$ (which are degenerate and correspond to ^5E_g in pseudo-D_{4h} symmetry) and $^5B_2$ ($^5B_{2g}$ in D_{4h} symmetry), with the state $^5B_2$ being the lowest one. A CI calculation based on the molecular orbitals obtained for the d^5 $^6A_{1g}$ $[Fe^{III}(P)(NH_3)_2]^+$ system leads to the conclusion that the ^5E_g state is the lowest state and that the character of the ^5E state is largely Fe(III) $e_g\pi^*$ with one electron transferred from the iron atom to the π system of the porphyrin ring. This result appears rather different from ours, and we tentatively attribute it to the fact that the reference wave function used in the CI calculation corresponds to an iron(III) system rather than to an iron(II) system. We feel that a meaningful comparison with our results is precluded for this reason.

In the work of Lecomte et al., it was found that a qualitative examination of the experimental deformation density maps and the multipole analysis on $FeTPP(THF)_2$ support either the $^5B_{1g}$ or the ^5E_g state, but these authors have concluded on qualitative grounds that the ^5E_g state must be the main contributor to the ground state of the complex, when covalent interactions are taken into account. On the other hand, our theoretical study cannot decide on energy grounds alone between the two states $^5B_{2g}$ and ^5E_g for $FeP(H_2O)_2$, but a comparison of the X–X, modelized, and theoretical maps in the porphyrin plane leaves no doubt about the ^5E_g state being the ground state. However, our interpretation of the double peak along the Fe–N bond does not rely on the covalent character of the Fe–N bond but on the contraction of the $d_{x^2-y^2}$ orbital due to the influence of σ donation. Except for $d_{x^2-y^2}$, the

(13) Rawlings, D. C.; Gouterman, M.; Davidson, E. R.; Feller, D. *Int. J. Quant. Chem.* **1985**, *28*, 797.

calculated iron d-orbital populations are in good agreement. However, one should keep in mind that the axial ligands are not identical in both studies (water versus THF) and that this may influence both the energy results and the electron distribution.

Acknowledgment. The calculations have been carried out on the CRAY computer of the CCVR (Palaiseau, France) through a grant of computer time from the Conseil Scientifique de Centre de Calcul Vectoriel pour la Recherche. We thank Professor Coppens for making his results available to us prior to publication.

Registry No. $FeP(H_2O)_2$, 122383-08-8.

Contribution from the Radiation Laboratory,
University of Notre Dame, Notre Dame, Indiana 46556

Photochemical Reactivity of the Cluster $Mo_6Cl_{14}^{2-}$: Photosubstitution and Photoredox Processes

B. Kraut and G. Ferraudi*

Received August 5, 1989

Photoreversible ligand substitution and ligand oxidation reactions have been observed in UV photolyses of $Mo_6Cl_{14}^{2-}$ in acetonitrile. The photosubstitution of the ligand detected in $\lambda_{excit} > 300$ nm takes place in competition with population of the low-lying states associated with $Mo_6Cl_{14}^{2-}$ phosphorescence and leads to the formation of intermediates that can be scavenged by excess cluster, Br^-, or I^-. The photoredox reaction, investigated by continuous and flash photolyses, has been detected for irradiation at wavelengths of the high energy charge transfer bands, $\lambda_{excit} < 300$ nm. Similar oxidations of the ligand have been observed in experiments where the large concentration of low-lying excited states induces excited-state disproportionation and excited-state photolysis, respectively. The mechanism of ligand photosubstitution is discussed in terms of the photophysical and photochemical properties of $Mo_6Cl_{14}^{2-}$ in irradiations with low and high intensities.

Introduction

The determination of the structure of molybdenum clusters, $Mo_6X_{14}^{2-}$, has shown that the nuclear configuration in these species consists of a nucleus of Mo atoms forming an octahedron while halide ions, X, occupy bridging and facial positions in a cubic array (I).[1-3] Metal-metal bonds in the complex have been described

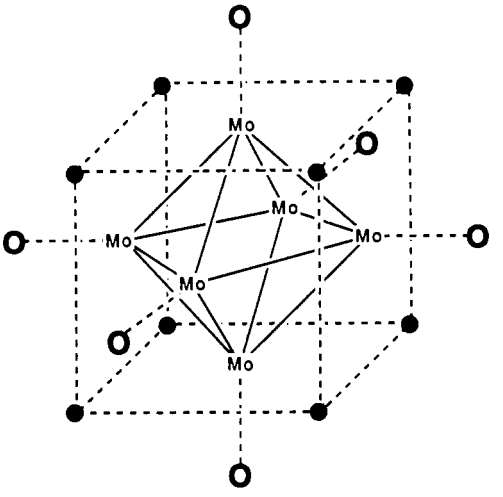

I

in terms of MO orbitals; the t_{2g} HOMO constructed by overlapping d_{xy} or d_{yz}, d_{xz} orbitals and the t_{1u} LUMO constructed by overlapping d_{z^2} orbitals.[4,5] These calculations have provided some quantitative information about the position of the electronic states. Moreover, recent studies on the photochemistry of these compounds have demonstrated that the luminescence is associated with three closely spaced excited states, which are subjected to rapid thermal equilibration (eq 1-3).[5]

$$(T_{1u})Mo_6Cl_{14}^{2-} \xrightarrow{13\ \mu s} Mo_6Cl_{14}^{2-} + h\nu' \quad (1)$$

$$Mo_6Cl_{14}^{2-} \xrightarrow{h\nu} (E_u)Mo_6Cl_{14}^{2-} \xrightarrow{185\ \mu s} Mo_6Cl_{14}^{2-} + h\nu'' \quad (2)$$

$$(T_{2u})Mo_6Cl_{14}^{2-} \xrightarrow{370\ \mu s} Mo_6Cl_{14}^{2-} + h\nu''' \quad (3)$$

$$Mo_6Cl_{13}^{-} + Cl^- \longrightarrow \cdots \quad (4)$$

This mixture of states, namely 65.2% T_{2u}, 28.9% E_u, and 5.9% T_{1u} relative Boltzmann populations at 298 K, gives rise to a long-lived phosphorescence, e.g. ca. 170 μs at 298 K in acetonitrile, which can be quenched by electron acceptors.[6-8] The ligand photosubstitution (eq 4) takes place by a path parallel to the formation of the photoemissive states and leads to the formation of reactive species that can be scavenged by halides or excess cluster.[9] In this work, the role of such intermediates in the photolysis of $Mo_6Cl_{14}^{2-}$ in CH_3CN has been investigated under conditions that we have previously used in sequential biphotonic excitations, e.g. high laser intensities and/or high concentration of complex.[10,11] Also, new photoredox reactions induced in photolyses with $\lambda_{excit} < 250$ nm are reported here.

Experimental Section

Photochemical Procedures. The apparatus used for flash photolysis and flash fluorescence experiments have been described elsewhere.[10-12] A flash lamp-pumped dye laser (Candela SLL-500 M) has been used for excitations at 440 nm. The output of the laser flash was varied by placing filters with appropriate optical densities in the light path. The light intensity was measured with a Scientech 365 power and energy meter. The solutions used for the flash experiments were deaerated with

(1) Brosset, C. *Ark. Kemi, Mineral. Geol.* **1945**, *20A*, No. 7.
(2) Brosset, C. *Ark. Kemi, Mineral. Geol.* **1947**, *25A*, No. 11.
(3) Vaughan, P. A. *Proc. Natl. Acad. Sci. U.S.A.* **1950**, *36*, 461.
(4) Zietlow, T. C.; Hopkins, M. D.; Gray, H. B. *J. Solid State Chem.* **1985**, *57*, 112.
(5) Saito, Y; Tanaka, H. K.; Sasaki, Y.; Azumi, T. *J. Phys. Chem.* **1985**, *89*, 4413.
(6) Maverick, A. W.; Gray, H. B. *J. Am. Chem. Soc.* **1981**, *103*, 1298.
(7) Maveric, A. W.; Najdzionek, J. S.; McKenzie, D.; Nocera, D. G.; Gray, H. B. *J. Am. Chem. Soc.* **1983**, *105*, 1878.
(8) Tanaka, H. K.; Sasaki, Y.; Saito, K. *Sci. Pap. Inst. Phys. Chem. Res. Jpn.* **1984**, *78*, 92.
(9) Kraut, B.; Ferraudi, G. Work in preparation.
(10) Van Vlierberge, B.; Ferraudi, G. *Inorg. Chem.* **1987**, *26*, 337.
(11) Van Vlierberge, B.; Ferraudi, G. *Inorg. Chem.* **1988**, *27*, 1386.
(12) Frink, M. E.; Geiger, D. K.; Ferraudi, G. *J. Phys. Chem.* **1986**, *90*, 1924.

0020-1669/89/1328-4578$01.50/0